Results in Physics 8 (2018) 16–25

Contents lists available at ScienceDirect

Results in Physics

journal homepage: www.journals.elsevier.com/results-in-physics

Effect of PbO on optical properties of tellurite glass

S.H. Elazoumi [a], H.A.A. Sidek [a,b,*], Y.S. Rammah [c], R. El-Mallawany [c], M.K. Halimah [a], K.A. Matori [a,b], M.H.M. Zaid [a,b]

[a] Physics Department, Faculty of Science, Universiti Putra Malaysia, 43400 UPM Serdang, Malaysia
[b] Materials Synthesis and Characterization Laboratory, Institute of Advanced Technology, Universiti Putra Malaysia, 43400 UPM Serdang, Selangor, Malaysia
[c] Physics Department, Faculty of Science, Menofia University, Egypt

ARTICLE INFO

Article history:
Received 21 June 2017
Received in revised form 14 September 2017
Accepted 9 November 2017
Available online 22 November 2017

Keywords:
Glass
Tellurite
Lead
Optical band gap
Urbach's energy

ABSTRACT

Binary $(1-x)(TeO_2)-x(PbO)$, x = 0, 0.10, 0.15, 0.20, 0.25, 0.30 mol% glass system was fabricated using melt quenching method. X-ray diffraction (XRD) technique was employed to confirm the amorphous nature. The microanalysis of the major components was performed using energy dispersive EDX and X-ray spectrometry. Both the molar volume and the density were measured. FTIR and UV spectra were recorded at 400–4000 cm^{-1} and 220–800 nm, respectively. The optical band gap (E_{opt}), Urbach's energy (E_u), index of refraction (n) were calculated using absorption spectrum fitting (ASF) and derivation of absorption spectrum fitting (DASF) methods. Molar refraction R_m and molecular polarizability α_m have been calculated according to (ASF) method.

Introduction

This article will introduce tellurite glasses as some smart materials because the world has entered the Glass Age. Tellurite glasses based on tellurium dioxide (TeO_2) are of technological interest due to their superior physical properties [1–20]. Recently, application of tellurite glasses has been achieved, especially in blue converted WLEDs, self cleanliness, and Pb-Te-O glasses affected silicon solar cells have been investigated [1,4]. A comparative study of the elastic, shielding and anomalous elastic and optical behavior in tellurite glasses have been measured [15–18]. Structure and optical band gap of $(PbO)_x(ZnO)_{10}(TeO_2)_{90-x}$ glasses have been measured [19].

The present objective is to measure the optical band gap energy (E_{opt}), Urbach's energy (E_u) and index of refraction (n). The value of n were calculated using the absorption spectrum fitting (ASF) and the derivation of absorption spectrum fitting (DASF) methods. Molar refraction R_m, molecular polarizability α_m, reflection loss (R_L) and optical transmission coefficient (T), metallization (M) and dielectric constant (ε) and ion Pb^{+2} and Oxygen packing density (O.P.D) have been calculated.

Experimental methods

The $(1-x)(TeO_2)-x(PbO)$ glasses; x = 0, 0.10, 0.15, 0.20, 0.25, 0.30 glass system was fabricated from high purity oxides mixed in specific weights, tellurium oxide TeO_2 (Alfa Aesar, 99.99%) and lead oxide PbO (Alfa Aesar, 99.99%). The homogenization of the 15 g of chemicals mixtures was effected by repeated grinding using a mortar for 30 min. The mixtures were preheated in a crucible (alumina crucible) at 280 °C for 1 h in an electric furnace. The preheated crucible was then moved to the another electrical furnace and kept for one hour at a temperature 850–900 °C. The molten mixture then turned into a cylindrically shaped stainless steel split mould preheated at 280 °C. After the quenching process, the solidified sample was then annealed at 280 °C for 1 h to avoid the mechanical strain developed during the quenching process and then the solidified glass is allowed to cool down to the room temperature. The samples of the glasses were cut into required dimension (between 6 to 10 mm) using the low-speed diamond blade to make great parallel surfaces for the measurements of ultrasonic velocities. Using a polishing machine with sand paper, the two sample's surfaces for each of the glasses were polished to get a plane parallelism. An X-ray diffraction (XRD) system was used to confirm the amorphousity or crystallinity of each sample by using an X-ray powder

* Corresponding author at: Physics Department, Faculty of Science, Universiti Putra Malaysia, 43400 UPM Serdang, Malaysia.
E-mail addresses: slazomi@gmail.com (S.H. Elazoumi), sidek@upm.edu.my (H.A.A. Sidek), dr_yasser1974@yahoo.com (Y.S. Rammah), raoufelmallawany@yahoo.com (R. El-Mallawany), hmk6360@gmail.com (M.K. Halimah), khamirul@upm.edu.my (K.A. Matori), mhmzaid@gmail.com (M.H.M. Zaid).

https://doi.org/10.1016/j.rinp.2017.11.010
2211-3797/

diffraction instrument (X'Pert Pro Panalytical PW 3040 MPD) in the range of (2θ) from 4° to 90° and energy dispersive EDX (Scanning Microscope, JSM.6400).

Density measurement of the glass sample was carried out using a densitometer model (MD-300S Densimeter). The density resolution was estimated around ±0.001 g/cm^3. For each of the samples, the density was measured using the following relationship:

$$\rho = \frac{W_{air}}{(W_{air} - W_{water})} \quad (1)$$

where (W_{air}) and (W_{water}) each representing the sample's weights, respectively in air and distilled water. Molar volume calculated from density using the equation, ($V_m = M_{glass}/\rho_{glass}$), where ρ_{glass} = glass sample density and M_{glass} = glass molecular weight.

For each glass sample, the molar volume determined by the expression below:

$$V_m = \frac{\sum_i x_i M_i}{\rho_{glass}} \quad (2)$$

where (M_i) is the molecular weight of an oxide component (i) and (x_i) is its mole fraction.

The FTIR spectra were obtained by using the FTIR spectrometer [400–4000 cm^{-1} & resolution of 0.85 cm^{-1} by KBr pellet technique] (Spectrum 100 perkin elmer). The UV absorption spectra of 0.2 cm thickness were measured in 220–800 nm using UV–Vis-NIR spectrophotometer (UV-3600 Shimadzu).

Results and discussion

Fig. 1 shows the photo of the prepared glasses are homogeneous and transparent. Fig. 2 shows the X-ray diffraction (XRD) pattern and confirm amorphous nature of $(1 - x)(TeO_2) - x(PbO$ glasses, x = 0, 0.10, 0.15, 0.20, 0.25, 0.30 mol%. Fig. 3a–f is the EDX spectrum, which only shows Te, Pb and O elements. EDX Analysis is a technique employed for identification of the elemental composition of a given specimen, or an area of interest. The profiles of the EDX analysis showed the presence of all the mentioned elements in the prepared samples. The prepared glass samples were homogeneous, lime green color and became more transparent as PbO increases as shown in Fig. 1. XRD pattern represents the confirmation that the present glasses are of amorphous nature as shown in Fig. 2. Also, Fig. 3a–f shows the EDX spectra for lead tellurite glass samples. It is observed from the result obtained that the use of alumina crucible induces a partial dissolution of Al_2O_3 in the melt that modifies the original composition.

The density (ρ), molar volume (V_m) and the OPD for the present glass system are collected in Table 1. Density of the glasses studied increased from 4930 to 6231 (kg/m^3), while molar volume decreased from 32.37 to 28.67 (cm^3/mol) as shown in Fig. 4. The glass density increase may be due to the high PbO molecular weight (223.1994) which is more than that of TeO_2 (159.6) and hence, the present glass matrix becomes more dense. Oxygen packing density decreased from 62.00 to 59.28 (mol/L) with the

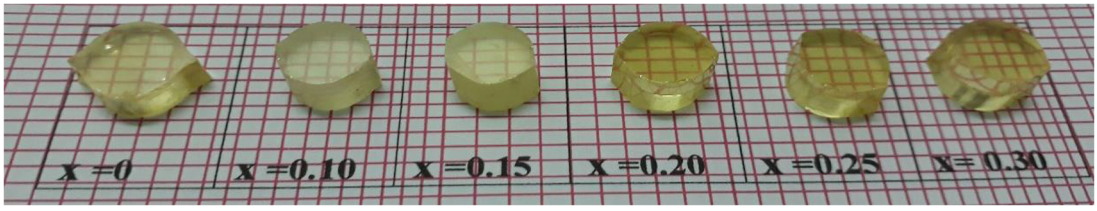

Fig. 1. Samples of $(1 - x)(TeO_2) - x(PbO)$ glasses, x = 0, 0.10, 0.15, 0.20, 0.25, 0.30 mol%.

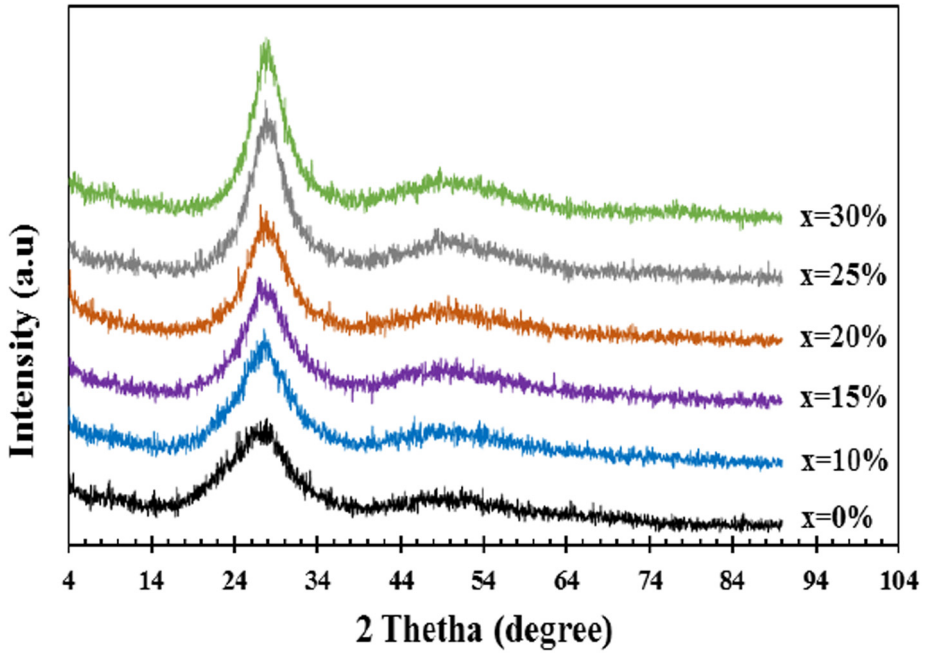

Fig. 2. X-ray diffraction (XRD) pattern of $(1 - x)(TeO_2) - x(PbO)$ glasses, x = 0, 0.10, 0.15, 0.20, 0.25, 0.30 mol%.

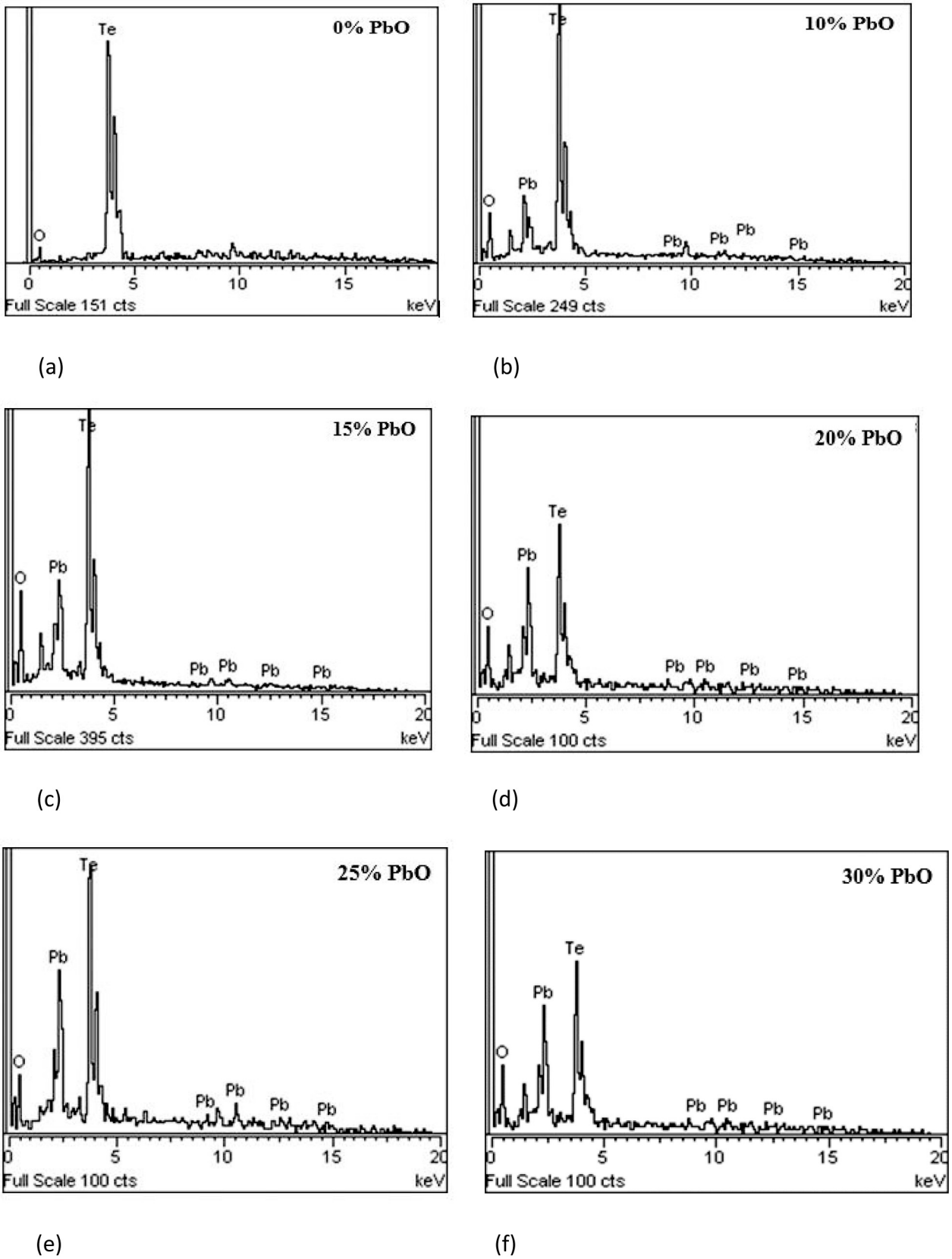

Fig. 3. (a–f): EDX pattern of $(1 - x)(TeO_2) - x(PbO)$ glasses, x = 0, 0.10, 0.15, 0.20, 0.25, 0.30 mol%.

substitution of PbO by TeO_2 as shown in Fig. 5. This attribute may be associated with the decrease in the number of oxygen atoms in a unit chemical composition.

FTIR spectrometry was utilized in obtaining important information about the structural units' arrangement of the present samples. The experimental FTIR spectra of the $(1 - x)(TeO_2) - x(PbO)$

Table 1
Density ρ, Molar volume V_m, indirect optical energy gap $E_{ASF}^{opt.}$, refractive index n, molar refraction R_m, and molecular polarizability α_m for glasses $(1-x)(TeO_2)-x(PbO)$, x = 0–30 PbO mole %.

Sample	Composition (*mol*%)		Density ρ	Molar Volume V_m	$E_{ASF}^{Opt.}$ indirect	n calculated indirect	R_m	α_m
	TeO_2	*PbO*	(kg m^{-3}) ± 10	(cm^3.mol^{-1}) ± 0.04	(eV)		(cm^3)	(10^{-24} cm^3)
S1	100	0	4930	32.37	2.65	2.49	23.43	9.29
S2	90	10	5371	30.89	2.72	2.47	22.23	8.82
S3	85	15	5611	30.14	2.62	2.50	21.87	8.67
S4	80	20	5843	29.49	2.87	2.43	20.96	8.32
S5	75	25	6048	29.02	2.70	2.48	20.91	8.30
S6	70	30	6231	28.67	2.38	2.58	21.22	8.42

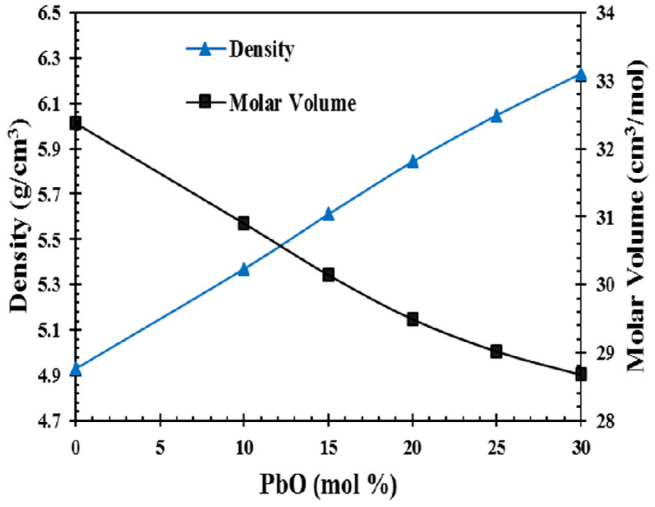

Fig. 4. Variation of density and molar volume of $(1-x)(TeO_2)-x(PbO)$, x = 0, 0.10, 0.15, 0.20, 0.25, 0.30 mol%.

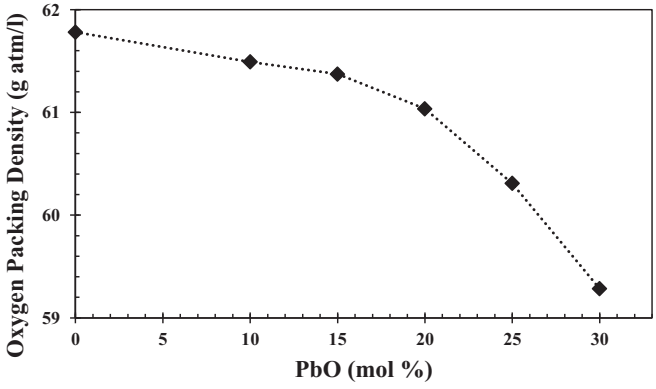

Fig. 5. Oxygen packing density of $(1-x)(TeO_2)-x(PbO)$, x = 0, 0.10, 0.15, 0.20, 0.25, 0.30 mol%.

glasses for different concentrations of lead oxide are presented in Fig. 6A. The result of FTIR shows the characteristics of chemical bond that exist between elements. Absorption peak in spectrum represents the frequencies of vibrations between the bonds of the atom or molecule. Tellurite oxide is characterised by two major structural configuration units; the trigonal bipyramid (TeO_4) and trigonal pyramid (TeO_3). Pure TeO_2 is characterised by an infrared absorption at around 640 cm^{-1} [20]. The band of absorption between 600–700 cm^{-1} represents the stretching vibration of the (Te-O) in the trigonal bipyramid (TeO_4) and trigonal pyramid (TeO_3) [21]. The stretching vibration of TeO_3 group is between 650–700 cm^{-1} while stretching vibration of TeO_4 which in between 600–650 cm^{-1} as in Table 2. In this work, Origin 8.0 software was used to observe that the concentration of TeO_4 increased as the concentration of PbO^{2+} ions increased from 0 to 0.10 mol indicating a decreasing non-bridging oxygen (NBO) number. Meanwhile, as the concentration of PbO^{2+} ions increases from 0.15 to 0.30 mol, TeO_4 concentration was seen to decrease steadily. The TeO_4 concentration increase indicates of the closely packed network in the glass caused by more bridging oxygens (BOs) formation. This trend is supported by the formation of trigonal pyramidal, structural units of TeO_3 within the glass system and causes a change of structural units from TeO_3 to TeO_4 with the formation of bridging oxygens as presented in Table 3 and Fig. 6B.

The UV–Vis spectra for glassy system $(1-x)(TeO_2)-x(PbO)$, x = 0–30 PbO mole % at 220–800 nm was presented in Fig. 7. With no sharp peaks in the optical absorption spectra confirms to characteristic of the studied glassy system that is amorphous in nature [28]. As the amount of lead oxide added into the glass system increases, one can observe the fundamental shifts in absorption to lower wavelength. This occurrence may be resulted from the increase in glass system rigidity as the lead oxide content increases. Optical energy band gaps for the present samples were determined using the method of ASF and DASF method. In these methods, the determination of the optical band gap energy is possible without the film thickness measurements and depends only on a measurement of the sample absorbance. According to our best knowledge, Tauc's formula [29] which modified by Mott and Davis can be expressed as [30]:

$$\alpha(\omega) = \frac{G(\hbar\omega - E^{Opt.})^m}{\hbar\omega} \tag{3}$$

where $\alpha(\omega)$ is the optical absorption coefficient which can be determined by Beer–Lambert's law. G, $\hbar\omega$, and $E_{Opt.}$ are a constant, energy of the incident photons, and the optical band gap energy, (m) is a constant that characterizes the optical transition type, which is respectively 1/2 or 2 for allowed direct or indirect transitions [29]. The optical coefficient of absorption, $\alpha(\omega)$ can be written as an incident photon wavelength (λ) function and Eq. (3) can be rewritten as [31,32]:

$$\alpha(\lambda) = G(hc)^{m-1}\lambda\left(\frac{1}{\lambda} - \frac{1}{\lambda_g}\right)^m \tag{4}$$

where $\alpha(\lambda)$ is absorption coefficient. h, c, and λ_g are the Planck's constant, light velocity, and wavelength corresponding to the optical gap, the velocity of the light, and Planck's constant, correspondingly. We can rewrite Eq. (4) as shown in Eq. (5):

$$A(\lambda) = D\lambda\left(\frac{1}{\lambda} - \frac{1}{\lambda_g}\right)^m \tag{5}$$

$D = [C(hc)^{m-1}\, d/2.303]$, where d is the sample thickness and A is the corresponding absorbance. Eq. (5) helps to determine optical band gap only by using the absorbance data avoiding sample thick-

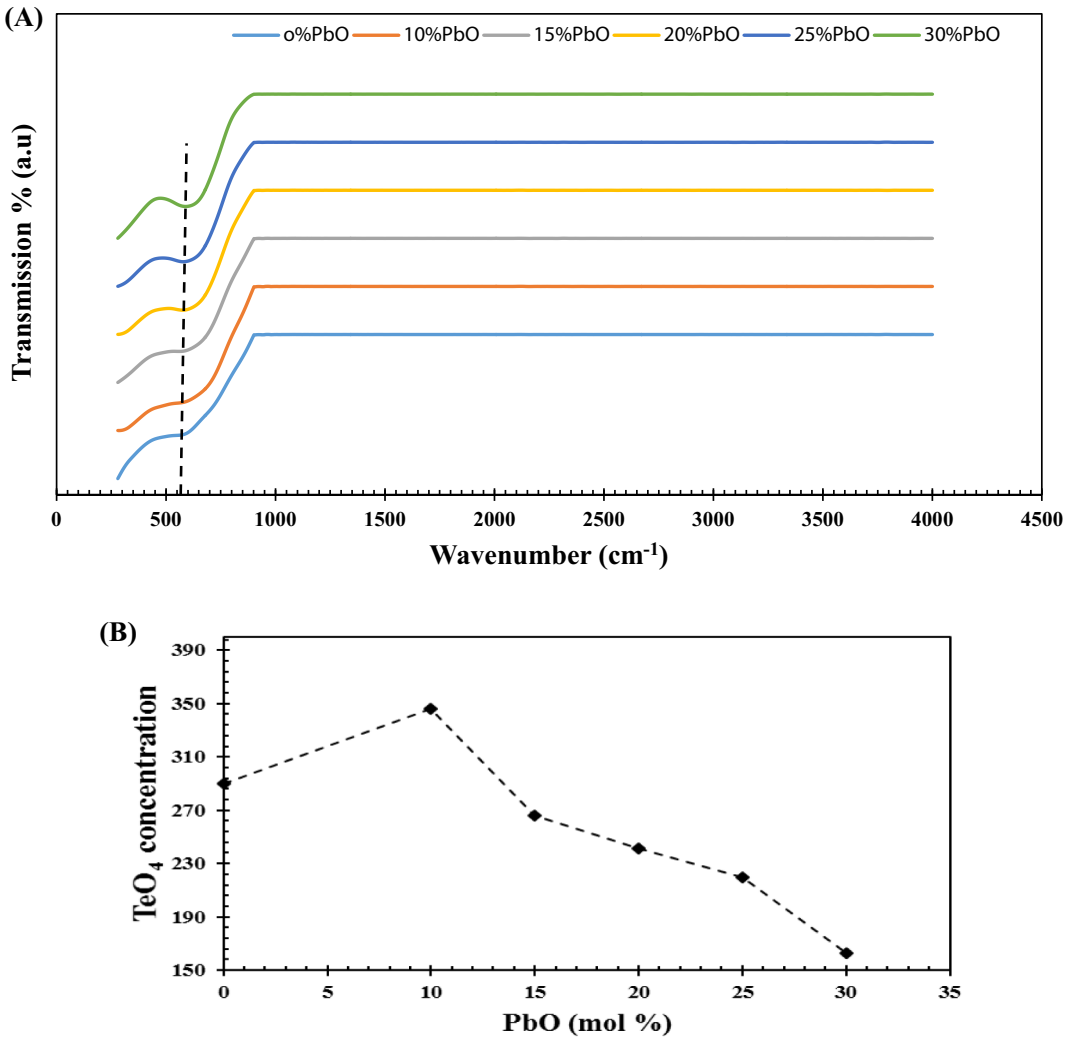

Fig. 6. (A, B): FTIR spectra and TeO4 concentration of $(1-x)(TeO_2)-x(PbO)$ glasses with x = 0, 0.10, 0.15, 0.20, 0.25, 0.30 mol%.

Table 2
Assignment of infrared transmission bands for $(1-x)(TeO_2)-x(PbO)$ glasses.

Wavenumber (cm^{-1})	Assignment	Refs.
480	Pb—O bonds vibrations in PbO_4 units	[22,23]
510	Pb—O symmetrical bending vibration	[22,23]
366–484	Te—O—Te or O—Te—O bending vibration	[22–24]
	Pb—O stretching vibrations in PbO_4 units	[25]
530–567	Pb—O symmetrical bending vibration	[22,23]
594–630	Te—O stretching vibration in TeO_4 units	[24–26]
664–677	Te—O bonds vibration in TeO_4 units	[26,22,27]
	Pb—O vibration in PbO n pyramidal units (n = 3 and/or 4)	
740–758	Te—O bonds vibration in TeO_3 units	[25]

Table 3
TeO_4 concentration of prepared glass sample with different concentration of lead oxide concentration.

X (mol%)	Area (TeO_4 Concentration)
0	290
10	346
15	266
20	241
25	220
30	163

ness. Therefore, the optical band gap energy can be determined directly from λ_g by:

$$E_{ASF}^{Opt.} = \frac{hc}{\lambda_g} = \frac{1239.83}{\lambda_g} \quad (6)$$

The value of λ_g can be deduced from extrapolation of the of $(A/\lambda)^{1/m}$ against (λ^{-1}) curve linear region where $(A/\lambda)^{1/m} = 0$. Figs. 8 and 9 represent the variation of $(A/\lambda)^2$ and $(A/\lambda)^{1/2}$ with $(1/\lambda)$ for direct and indirect allowed transition, respectively for glassy system $(1-x)(TeO_2)-x(PbO)$, x = 30 PbO mole %. The rest of samples follow the same behavior and values of $E_{ASF}^{opt.}$ are tabulated in Table 1. The energy gap values for both transitions (direct and indirect) decrease with increasing value of PbO content. Moreover, the values of energy gaps in the indirect case are smaller than that of direct one as shown in Fig. 10. Also, the optical energy band gaps in the present glass system were determined using the DASF method [32]. Fig. 11(A and B) depicts the plots of $d\{\ln[A(\lambda)\lambda^{-1}]\}/d\lambda^{-1}$ versus (λ^{-1}) for the base glass (0.0% PbO) and the glass of (30% PbO), respectively. The optical energy gap has been calculated using the following relation [32]:

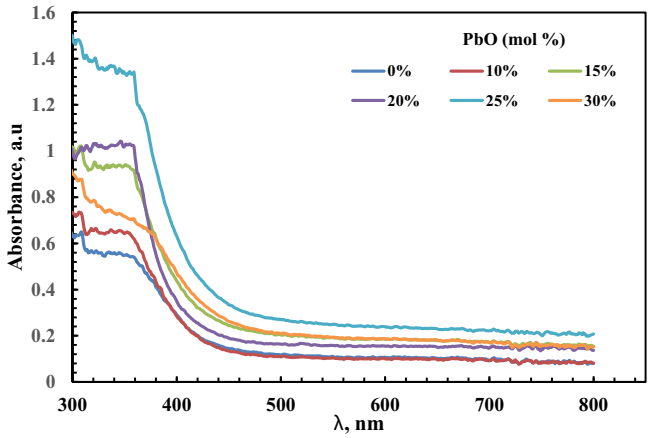

Fig. 7. UV absorption spectra of $(1 - x)(TeO_2) - x(PbO)$ glass, x = 0–30 PbO mole %.

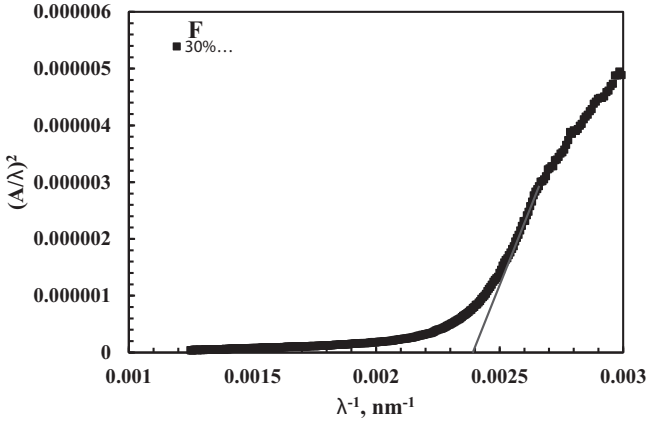

Fig. 8. Variation of $(A/\lambda)^2$ with (λ^{-1}) for $(1 - x)(TeO_2) - x(PbO)$ glass, x = 30 PbO mole %.

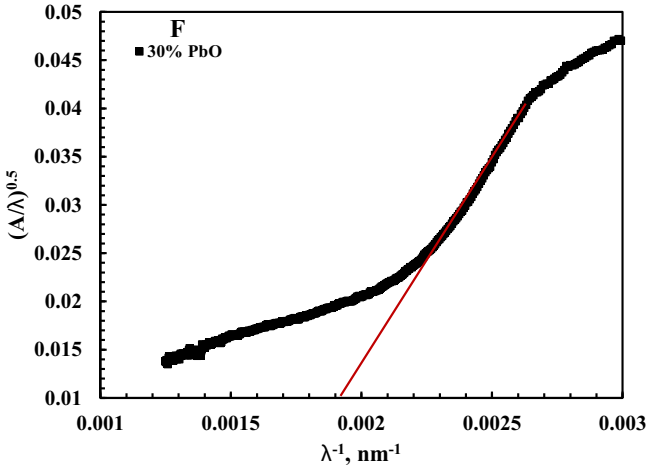

Fig. 9. Variation of $(A/\lambda)^{0.5}$ with (λ^{-1}) for $(1 - x)(TeO_2) - x(PbO)$ glass, x = 30 PbO mole %.

$$E_{DASF}^{Opt.} = \frac{hc}{\lambda_g} = \frac{1239.83}{\lambda_g} \tag{7}$$

The obtained energy gap values for the studied glass samples using DASF model were listed in Table 4. Results indicate that there is a good agreement between energy gap values which obtained

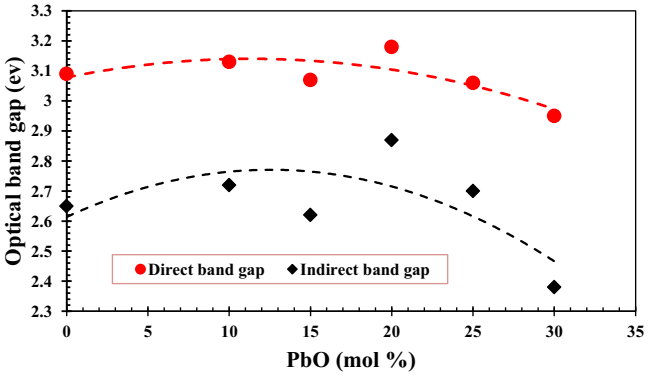

Fig. 10. Energy gap values for $(1 - x)(TeO_2) - x(PbO)$ glass, x = 0–30 PbO mole %.

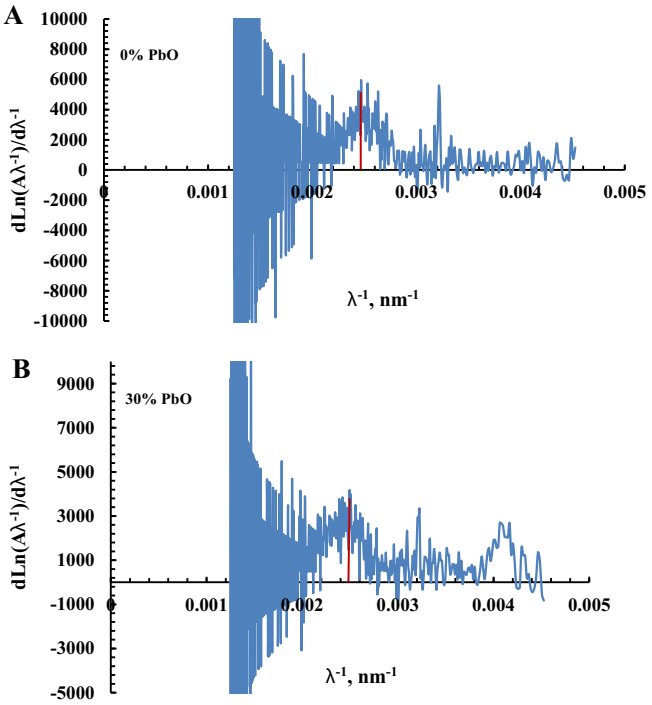

Fig. 11. Variation of $d\{\ln[A(\lambda)/\lambda]\}/d(1/\lambda)$ versus $(1/\lambda)$ for the base glass: (A) 0.0 % PbO and (B) 30% PbO.

from ASF, DASF methods and values obtained from Tauc's model (figures not shown here).

Refractive index of $(1 - x)(TeO_2)x(PbO)$, x = 0–30 PbO mole % glass systems was determined by the following equation [33,34]:

$$\left(\frac{n^2 - 1}{n^2 + 2}\right) = 1 - \left(\frac{E^{Opt.}}{20}\right)^{1/2} \tag{8}$$

The calculated refractive index by both ASF and DASF methods collected in Table 4 and represented in Fig. 12. Results showed that the refractive index of all samples is considerably high.

Molar refraction (R_m), polarizability (α_m), reflection loss (R_L), and optical transmission (T)

Molar refraction is the degree of the total polarizability per unit mole of material. Lorentz-Lorenz equation is used to relate the molar refractivity, R_m to index of refraction, n and molar volume, V_m as the equation below presents [35,36]:

Table 4
The ($E^{opt.}$), and (n) by Tauc's, ASF, and DASF methods for glasses (1 – x)(TeO_2) – x(PbO), x = 0–30 PbO mole %.

x PbO (mol%)	$E^{Opt}_{Tauc's}$(eV) by Tauc's method		$E^{Opt.}_{ASF}$ (eV) by ASF method		$E^{Opt.}_{DASF}$ (eV) by DASF method	Refractive index, n Tauc's method	Refractive index, n ASF method	Refractive index, n DASF method
	Direct	Indirect	Direct	Indirect				
0	3.11	2.80	3.09	2.65	3.06	2.45	2.49	2.38
10	3.21	3.00	3.13	2.72	3.02	2.39	2.47	2.39
15	3.20	2.91	3.07	2.62	2.97	2.42	2.50	2.40
20	3.19	2.88	3.18	2.87	3.35	2.43	2.43	2.30
25	3.13	2.77	3.06	2.70	3.18	2.46	2.48	2.34
30	2.94	2.65	2.95	2.38	3.09	2.49	2.58	2.37

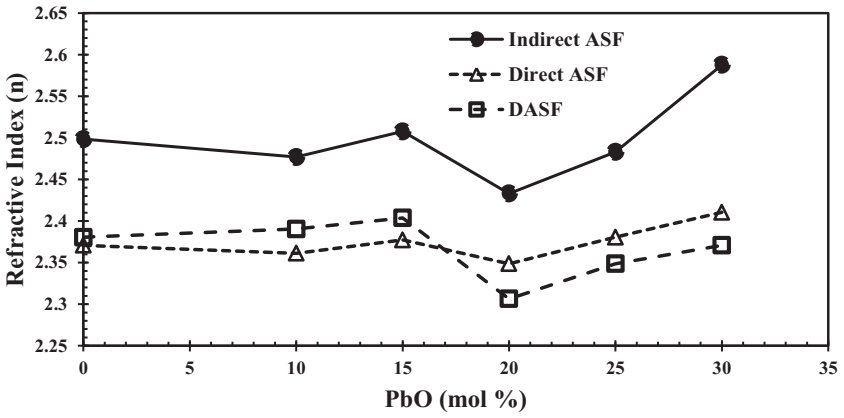

Fig. 12. Refractive index for glasses (1 – x)(TeO_2) – x(PbO) glass, x = 0–30 PbO mole %.

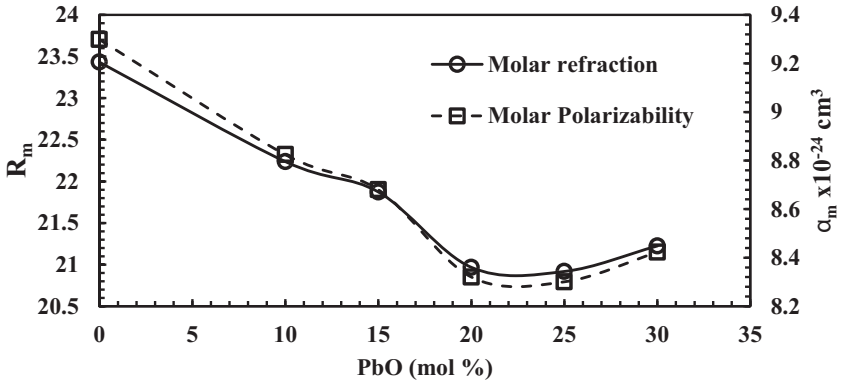

Fig. 13. Molar refraction R_m and molecular polarizability α_m for (1 – x)(TeO_2) – x(PbO) glass, x = 0–30 PbO mole %.

$$R_m = \left(\frac{n^2-1}{n^2+2}\right)\frac{M_{glass}}{\rho_{glass}} = \left(\frac{n^2-1}{n^2+2}\right)V_m \quad (9)$$

where R_m, M_{glass}, ρ_{glass}, V_m, and n are respectively the molar refraction, the molar mass, the density, the molar volume, and index of refraction of the glass sample. Eq. (9) provides the average molar refraction for substances that are isotropic in nature, such as cubic crystals, liquids and glasses.

The molar refractivity can also be expressed as a function of electronic polarizability α_m of a molecule, which is the magnitude of electrons responds to an electric field as [36,37]:

$$R_m = 2.52\alpha_m \quad (10)$$

Table 1 summarized the density (ρ) values, Molar volume V_m, indirect optical energy gap $E^{opt.}_{ASF}$, the corresponding index of refraction (n), molar refractivity (R_m), and molar polarizability (α_m) for glass system (1 – x)(TeO_2) – x(PbO), x = 0–30 PbO mole %. Fig. 13 plots the relation between the calculated values for molar refraction and electronic polarizability as a function of PbO content in glassy system (1 – x)(TeO_2) – x(PbO), x = 0–30 PbO mole %. It is clear that both of R_m and α_m has a decreasing trend, this may be occurred due to the decreasing number of NBO in the fabricated glass system as the concentration of PbO increases. Nonbridging oxygen has high tendency to polarize compared with bridging oxygen [38]. Thus the studied glasses tend to be less polarized.

Reflection loss, R_L and optical transmission, T for the fabricated glass system (1 – x)(TeO_2)x(PbO), x = 0–30 PbO mol% were calculated through Eqs. (11) and (12), respectively:

$$R_L = \left(\frac{n-1}{n+1}\right)^2 \quad (11)$$

$$T = \frac{2n}{n^2+1} \quad (12)$$

The calculated reflection loss R_L and optical transmission T for the present glasses are collected in Table 5 and illustrated in Fig. 14. Results show that R_L and T have an inverse behavior with PbO concentration.

Metallization criterion (M) and dielectric constant (ε)

According to the metallization theory for condensed matter as Herzfeld [39], metallization criterion (M) is theoretically calculated to estimate the tendency for metallization and to investigate the insulating behavior of the fabricated glasses. This theory explained that the refractive index becomes infinite under the condition that $R_m/V_m = 1$ in the above Lorentz-Lorenz equation, which correlates with the covalent solid materials metallization. This means that the electron gets itinerant and the glasses become metallic in nature. Predicting of the metallic nature or otherwise of solids depends on the necessary and sufficient condition which is [40,41]:

$$\frac{R_m}{V_m} > 1, \quad \text{for metallic nature, and}$$

$$\frac{R_m}{V_m} < 1, \quad \text{for non-metallic nature}$$

The metallization criterion, M for the studied glasses were obtained by subtracting the ratio R_m/V_m by 1 [42]:

$$M = 1 - \left(\frac{R_m}{V_m}\right) \tag{13}$$

In addition, the dielectric constant (ε) for $(1 - x)(TeO_2) - x$ (PbO), x = 0–30 PbO mole % was calculated by [43]:

$$\varepsilon = n^2 \tag{14}$$

The values of metallization criterion M and dielectric constant ε for the present glasses are calculated using Eqs. (13) and (14), then

Table 5
Reflection loss R_L, optical transmission T, metallization criterion M, dielectric constant ε, refractive index based metallization criterion M(n), and energy band gap based metallization criterion $M(E^{Opt.})$ for glasses $(1 - x)(TeO_2) - x$(PbO), x = 0–30 PbO mole %.

Sample	Composition (*mol%*)		R_L	T	M	ε	$M(n)$	$M(E^{Opt.})$
	TeO₂	***PbO***						
S1	100	0	0.183	0.689	0.276	6.24	0.364	0.364
S2	90	10	0.180	0.694	0.280	6.13	0.368	0.368
S3	85	15	0.184	0.688	0.274	6.28	0.361	0.361
S4	80	20	0.174	0.703	0.284	5.19	0.378	0.378
S5	75	25	0.181	0.693	0.279	6.16	0.367	0.367
S6	70	30	0.195	0.672	0.259	6.69	0.344	0.344

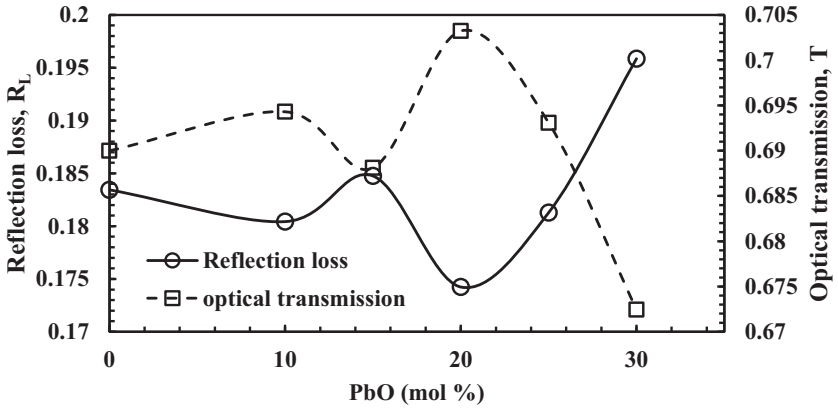

Fig. 14. Reflection loss R_L and optical transmission T for $(1 - x)(TeO_2) - x$(PbO) glass, x = 0–30 PbO mole %.

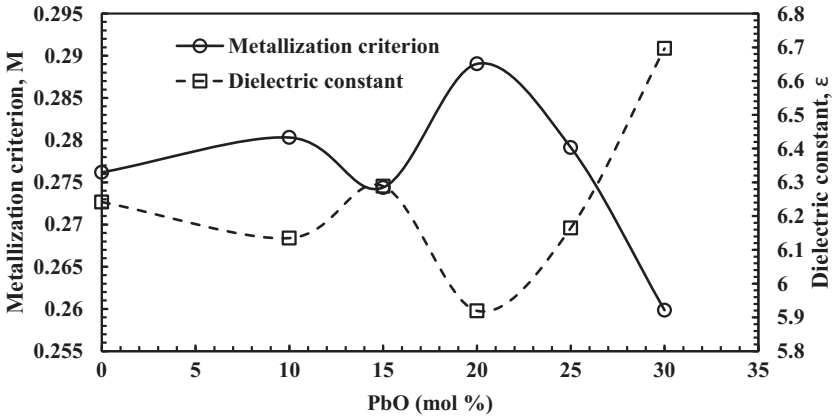

Fig. 15. Metallization criterion M and dielectric constant ε for $(1 - x)(TeO_2) - x$(PbO) glass, x = 0–30 PbO mole %.

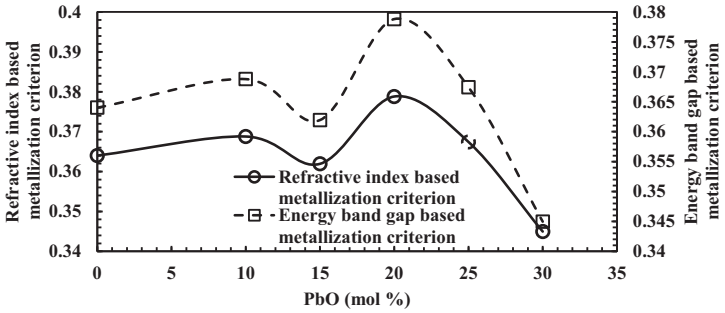

Fig. 16. Refractive index and energy band gap based metallization criterion of $(1-x)(TeO_2)-x(PbO)$ glass, x = 0–30 PbO mole %.

tabulated in Table 3 and plotted against the PbO concentration as shown in Fig. 15**.** Results show that the behavior of metallization criterion and dielectric constant for the glassy system $(1-x)(TeO_2)-x(PbO)$, x = 0–30 PbO mole % is inversely with PbO content.

Metallization criterion based on index refraction $M(n)$ and optical energy band gap $M(E^{Opt.})$ have been calculated using the equations below [42]:

$$M(n) = 1 - \left(\frac{n^2-1}{n^2+2}\right) \tag{15}$$

$$M(E^{Opt.}) = \left(\frac{E^{Opt.}}{20}\right)^{1/2} \tag{16}$$

The $M(n_o)$ and $M(E^{Opt.})$ values for the system $(1-x)(TeO_2)-x(PbO)$, x = 0–30 PbO mole % were calculated using Eqs. (15) and (16) are listed in Table 3 and plotted against PbO concentration in Fig. 16. Both the energy band gap based and refractive index based metallization criterion has the same trend, increases with the increasing PbO amount indicates a decreasing chance of metallization in the electronic structure of the fabricated system of glass with increasing PbO content. In addition, the increasing trend in metallization criterion on the basis of band gap energy indicates that the samples are not metalizing and the width of conduction bands becomes smaller, these results in more agreement with previous work [44]. Also, recently more application of tellurite glasses has been established [45,46].

Conclusions

Homogeneous and transparent $(1-x)(TeO_2)-x(PbO)$ glasses where x = 0, 0.10, 0.15, 0.20, 0.25, 0.30 mol% have been achieved and found that:

- EDX spectra confirmed that alumina crucible induces a partial dissolution of Al_2O_3 in the melt that modifies the original composition. The Al_2O_3 contamination is around 6 to 7%.
- Densities of the glass system studied are generally high and tend to increase from 4930 to 6231 kg/m^3 for 0 to 30 mol% PbO.
- Molar volume decreased from 32.37 to 28.68 (cm^3/mol) with the mole percentage of PbO.
- The main characteristics of the FTIR spectra of the base glass exhibited the main absorption band at 600 cm^{-1} which are attributed to the different structural units of TeO_2, PbO.
- The optical band gap was decreased due to increase in the number of (NBO) and the rigidity.
- Refractive index increases with increase of PbO due to decrease in the optical energy gap.
- The behavior of metallization criterion and dielectric constant for the glassy system studied is inversely with PbO content.

Acknowledgement

The researchers acknowledged with gratitute the financial support for this work by the Malaysian Ministry of Higher Education (MOHE) and Universiti Putra Malaysia through the Fundamental Research Grant Scheme (FRGS) and Inisiatif Putra Berkumpulan (IPB) research grant.

References

[1] Yu C, Yang Z, Huang A, Chai Z, Qiu J, Song Z, et al. Photoluminescence properties of tellurite glasses doped Dy^{3+} and Eu^{3+} for the UV and blue converted WLEDs. J Non-Cryst Solids 2017;457:1–8.
[2] El-Mallawany R. Quantitative analysis of elastic moduli of tellurite glasses. J Mater Res 1990;5:2218–22.
[3] El-Mallawany R. Devitrification and vitrification of tellurite glasses. J Mater Sci Electron 1995;6:1–3.
[4] Nurhafizah H, Rohani MS, Ghoshal SK. Self cleanliness of Er^{3+}/Nd^{3+} Co-doped lithium niobate tellurite glass containing silver nanoparticles. J Non-Cryst Solids 2017;455:62–9.
[5] Hagar I, El-Mallawany R, Poulain M. Infrared and Raman spectra of new molybdenum and tungsten oxyfluoride glasses. J Mater Sci Lett 1999;34:5158–68.
[6] El-Mallawany R, Sidky M, Kafagy A, Afifi H. Elastic constants of semiconducting tellurite glasses. Mater Chem Phys 1994;37:295–8.
[7] Souri D. Suggestion for using the thermal stable thermoelectric glasses as a strategy for improvement of photovoltaic system efficiency: Seebeck coefficients of tellurite-vanadate glasses containing antimony oxide. Sol Energy. 2016;139:19–22.
[8] Sidkey MA, ElMallawany RA, Abousehly AA, Saddeek YB. Relaxation of longitudinal ultrasonic waves in some tellurite glasses. Mater Chem Phys 2002;74:222–9.
[9] El-Mallawany R, Sidkey M, Khafagy A, Afifi H. Ultrasonic attenuation of tellurite glasses. Mater Chem Phys 1994;37:197–200.
[10] Abdel Kader A, El-Mallawany R, ElKholy M. Network structure of tellurite phosphate glasses: optical absorption and ir spectra. J Appl Phys 1993;73:71.
[11] Hager IZ, El-Mallawany R. Preparation and structural studied in the (70-x) TeO_2-20WO_3-10Li_2O-xLn_2O_3 glasses. J Mater Sci 2010;45:897–905.
[12] Moawad HM, Jain H, El-Mallawany R, Ramadan T, El-Sharbiny M. Electrical conductivity of silver vanadium tellurite glasses. J Am Ceram Soc 2002;85:2655–9.
[13] Qin J, Zhang W, Bai S, Liu Z. Effect of Pb-Te-O glasses on Ag thick-film contact in crystalline silicon solar cells. Sol Energy Mater Sol Cells 2016;144:256–63.
[14] Hager I, El-Mallawany R, Bulou A. Luminescence spectra and optical properties of TeO_2–WO_3–Li_2O glasses doped with Nd, Sm and Er rare earth ions. Physica B 2011;406:972–80. and Idem, ibid, 406 (2011) 1844.
[15] Hasnimulyati L, Halimah MK, Zakaria A, Halim SA, Ishak M. A comparative study of the experimental and the theoretical elastic data of Tm^{3+} doped zinc borotellurite glass. Mater Chem Phys 2017;192:228–34.
[16] Sidek HAA, El-Mallawany R, Matori KA, Halimah MK. Effect of PbO on the elastic behavior of ZnO–P_2O_5 glass systems. Results Phys 2016;6:449–55.
[17] Matori KA, Sayyed MI, Sidek HAA, Zaid MHM, Singh VP. Comprehensive study on physical, elastic and shielding properties of lead zinc phosphate glasses. J Non-Cryst Solids 2017;457:97–103.
[18] Khanisanij M, Sidek HAA. Elastic behavior of borate glasses containing lead and bismuth oxides. Adv Mater Sci Eng 2014;2014:1–8.
[19] Ticha H, Schwarz J, Tichy L. On the structural arrangement and optical band gap (PbO)x(ZnO)10(TeO_2)90 – x glasses. J Non-Cryst Solids 2017;459:63–7.
[20] Gayathri Pavani P, Sadhana K, Chandra Mouli V. Optical, physical and structural studies of boro-zinc tellurite glasses. Physica B 2011;406:1242–7.
[21] Azlan MN, Halimah MK, Shafinas SZ, Daud WM. Physics, influence of erbium concentration on spectroscopic properties of tellurite. Solid State Sci Technol 2014;22:148–56.

[22] Bosca M, Pop L, Borodi G, Pascuta P, Culea E. XRD and FTIR structural investigations of erbium-doped bismuth-lead-silver glasses and glass ceramics. J Alloy Compd 2009;479:579–82.
[23] Rada S, Dehelean A, Culea E. FTIR and UV-VIS spectroscopy investigations on the structure of the europium-lead-tellurate glasses. J Non-Cryst Solids 2011;357:3070–3.
[24] Culea E. Structural and magnetic behaviour of lead-bismuthate glasses containing rare earth ions. J Non-Cryst Solids 2011;357:50–4.
[25] Mansour E. FTIR spectra of pseudo-binary sodium borate glasses containing TeO_2. J Mol Struct 2012;1014:1–6.
[26] Mohamed EA, Ahmad F, Aly KA. Effect of lithium addition on thermal and optical properties of zinc-tellurite glass. J Alloy Compd 2012;538:230–6.
[27] Çelikbilek M, Ersundu AE, Aydin S. Preparation and characterization of TeO_2–WO_3–Li_2O glasses. J Non-Cryst Solids 2013;378:247–53.
[28] Pavani PG, Suresh S, Mouli VC. Studies on boro cadmium tellurite glasses. Opt Mater 2001;34:215–20.
[29] Zaid MHM, Matori KA, Quah HJ, Lim WF, Sidek HAA, Halimah MK, Yunus WMM, Wahab ZA. Investigation on structural and optical properties of SLS-ZnO glasses prepared using a conventional melt quenching technique. J Mater Sci-Mater El 2015;26:3722–9.
[30] Mott NF, Davies EA. Electronic processes in non-crystalline materials. Oxford: Clarendon Press; 1979.
[31] Alarcon LE, Arrieta A, Camps E, Muhl S, Rudil S, Santiago EV. An alternative procedure for the determination of the optical band gap and thickness of amorphous carbon nitride thin films. Appl Surf Sci 2007;254:412–5.
[32] Souri D, Tahan ZE. A new method for the determination of optical band gap and the nature of optical transitions in semiconductors. Appl Phys B 2015;119:273–9.
[33] Dimitrov V, Sakka S. Electronic oxide polarizability and optical basicity of simple oxides. J Appl Phys 1996;79:1736–40.
[34] El-Mallawany R, Dirar Abdalla M, Abbas Ahmed I. New tellurite glasses: optical properties. Mater Chem Phys 2008;109:291–6. and QNRS Repository (1) (2011) 1048.
[35] Moelwyn-Hughes EA. Physical chemistry. London: Pergamon; 1961.
[36] El-Mallawany R. Optical properties of tellurite glasses. J Appl Phys 1992;72:1774–7.
[37] Rawson H. Properties and applications of glass. Amsterdam: Elsevier; 1980.
[38] Azlan MN, Halimah MK, Shafinas SZ, Daud WM. Electronic polarizability of zinc borotellurite glass system containing erbium nanoparticles. Mater Exp 2015;5:211–8.
[39] Herzfeld KF. On atomic properties which make an element a metal. Phys Rev 1927;29:701–5.
[40] Honma T, Sato R, Benino Y, Komatsu T, Dimitrov V. Electronic polarizability, optical basicity and XPS spectra of Sb2O3–B2O3 glasses. J Non-Cryst Solids 2000;272:1–13.
[41] Azlan MN, Halimah MK, Shafinas SZ, Daud WM. Polarizability and optical basicity of Er^{3+} ions doped tellurite based glasses. Chalcogenide Lett 2014;11:319–35.
[42] Dimitrov V, Sakka S. Linear and nonlinear optical properties of simple oxides. II. J Appl Phys 1996;79:1741–5.
[43] Wakkad MM, Shokr EKh, Mohamed SH. Optical and calorimetric studies of Ge–Sb–Se glasses. J Non-Cryst Solids 2000;265:157–66.
[44] Dimitrov V, Komatsu T. An interpretation of optical properties of oxides and oxide glasses in terms of the electronic ion polarizability and average single bond strength. J Univ Chem Technol Metall 2010;45:219–50.
[45] El-Mallawany R, Sayyed MI, Dong MG. Comparative shielding properties of some tellurite glasses: part 2. J Non-Cryst Solids 2017;474:16–23.
[46] Sayyed1 MI, El-Mallawany R. Shielding properties of $(100\text{-}x)TeO_2$–$(x)MoO_3$ glasses. Mater Chem Phys 2017;201:50–6.